4-21-2008

Slip Boundary Conditions for Shear Flow of Polymer Melts Past Atomically Flat Surfaces

Anoosheh Niavarani

Nikolai V. Priezjev
Wright State University - Main Campus, nikolai.priezjev@wright.edu

Slip boundary conditions for shear flow of polymer melts past atomically flat surfaces

Anoosheh Niavarani and Nikolai V. Priezjev

Department of Mechanical Engineering,

Michigan State University, East Lansing, Michigan 48824

(Dated: November 4, 2018)

Abstract

Molecular dynamics simulations are carried out to investigate the dynamic behavior of the slip length in thin polymer films confined between atomically smooth thermal surfaces. For weak wall-fluid interactions, the shear rate dependence of the slip length acquires a distinct local minimum followed by a rapid growth at higher shear rates. With increasing fluid density, the position of the local minimum is shifted to lower shear rates. We found that the ratio of the shear viscosity to the slip length, which defines the friction coefficient at the liquid/solid interface, undergoes a transition from a nearly constant value to the power law decay as a function of the slip velocity. In a wide range of shear rates and fluid densities, the friction coefficient is determined by the product of the value of surface induced peak in the structure factor and the contact density of the first fluid layer near the solid wall.

I. INTRODUCTION

The fluid flow in microfluidic channels can be significantly influenced by liquid slip at the solid boundary because of the large surface to volume ratio [1]. The Navier model for the partial slip boundary conditions relates the fluid slip velocity to the tangential viscous stress at the wall via the friction coefficient, which is defined as the ratio of the shear viscosity to the slip length. Geometrically, the slip length is determined as a distance from the solid wall where the linearly extrapolated fluid velocity profile vanishes. Experimental studies have demonstrated that for atomically smooth surfaces the slip length is relatively large for non-wetting liquid/solid interfaces [2, 3, 4], polymeric fluids [5, 6] and high shear rates [7, 8, 9]. By contrast, surface roughness even on the submicron length scale strongly reduces the degree of slip for both polymeric [10] and Newtonian [11, 12, 13] fluids. However, experimentally it is often difficult to isolate and, consequently, to analyze the effects of wettability, surface roughness and shear rate on slip boundary conditions because of the small scales involved.

During the past two decades, a number of molecular dynamics (MD) simulations [14, 15, 16, 17, 18, 19, 20, 21, 22, 23] have been performed to investigate the dependence of the slip length on the structure of dense fluids near atomically flat surfaces. For simple fluids, it has been well established that the slip length correlates inversely with the wall-fluid interaction energy and the surface induced order in the first fluid layer [15, 16, 23]. The strong wall-fluid coupling and commensurate structures of the liquid/solid interface lead to the no-slip boundary condition for monoatomic fluids [15, 21]. The interfacial slip is enhanced in the flow of polymer melts due to the higher shear viscosity and reduced molecular ordering near the flat wall [20, 24, 25, 26]. The magnitude of the slip length in the flow of polycarbonate blends past atomically smooth nickel surfaces is determined by the competition between the apparent slip of the adsorbed polymer layer and its thickness [27]. The slip boundary conditions for the polymer melt flow over the brush can be controlled by changing the density of the end-grafted polymer layer [28]. Finally, the degree of slip at the interface between immiscible polymers is larger for longer chain molecules and greater repulsion between unlike species [29].

Until ten years ago, the slip length in the Navier model was assumed to be independent of shear rate. In the seminal MD study by Thompson and Troian [30] on shear flow of simple fluids past atomically flat rigid walls, it was found that the slip length increases nonlinearly

with the shear rate. Upon increasing the surface energy, a gradual transition from the power law behavior [30] to the linear rate dependence was recently reported for weak wall-fluid interactions and incommensurate structures of the liquid/solid interface [23]. In a wide range of shear rates and surface energies, the slip length in simple fluids is determined by a function of the in-plane structure factor, contact density and temperature of the first fluid layer near the wall [23]. The rate-dependent slip length at the interface between a polymer melt composed of short linear chains and a crystalline substrate is also well described by the power law function used to fit the data for simple fluids [20, 30]. Whether these boundary conditions hold for higher molecular weight polymers or rough surfaces is an open question that has to be addressed for the correct interpretation of the experimental results and modeling fluid flows in microfluidic channels.

In this paper, the effects of shear rate and fluid density on slip boundary conditions for the flow of a polymer melt past a crystalline wall are investigated by molecular dynamics simulations. We will show that the rate-dependent slip length reaches a local minimum and then increases rapidly at higher shear rates. In the shear thinning regime, the friction coefficient at the liquid/solid interface follows a power law decay as a function of the slip velocity. In a wide range of shear rates and polymer densities, the ratio of the slip length to the shear viscosity is determined by the surface induced structure in the first fluid layer. These results suggest that the correlation between the fluid structure near the flat wall and the slip length is determined by a universal combination of parameters for both polymer melts and simple fluids [23].

This paper is organized as follows. The molecular dynamics simulation model and parameter values are described in the next section. The results for the rate dependence of the slip length and the analysis of the fluid structure near the solid wall are presented in Section III. The conclusions are given in the last section.

II. DETAILS OF MOLECULAR DYNAMICS SIMULATIONS

The polymer melt is confined between two atomically flat walls and is subject to planar shear in the $\hat{x}$ direction (see Fig. 1 for a schematic representation). The fluid monomers interact through the pairwise Lennard-Jones (LJ) potential

$$V_{LJ}(r) = 4\,\varepsilon \left[\left(\frac{\sigma}{r}\right)^{12} - \left(\frac{\sigma}{r}\right)^{6} \right], \tag{1}$$

with a cutoff distance $r_c = 2.5\,\sigma$, where ε and σ represent the energy and length scales of the fluid phase. The total number of monomers is $N_f = 6000$. The wall-fluid interaction parameters of the LJ potential are set to $\varepsilon_{\rm wf} = 0.9\,\varepsilon$ and $\sigma_{\rm wf} = \sigma$ throughout the study. The polymer melt is modeled as a collection of bead-spring chains of $N = 20$ LJ monomers interacting through the FENE (finitely extensible nonlinear elastic) potential [31]

$$V_{FENE}(r) = -\frac{k}{2}\, r_o^2 \ln[1 - r^2/r_o^2], \tag{2}$$

with Kremer and Grest parameters $k = 30\,\varepsilon\sigma^{-2}$ and $r_o = 1.5\,\sigma$ [32]. This choice of parameters prevents polymer chains from unphysical crossing or bond breaking [33].

The system was coupled to an external heat bath through a Langevin thermostat [33] with a random force and a damping term with a small value of the friction coefficient $\Gamma = 1.0\,\tau^{-1}$ [34]. The thermostat was only applied to the equation of motion for a fluid monomer along the $\hat{y}$ axis to avoid a bias in the shear flow direction [15]. The equations of motion for the $\hat{x}$, $\hat{y}$ and $\hat{z}$ components are given by

$$m\ddot{x}_i = -\sum_{i\neq j} \frac{\partial V_{ij}}{\partial x_i}\,, \tag{3}$$

$$m\ddot{y}_i + m\Gamma\dot{y}_i = -\sum_{i\neq j} \frac{\partial V_{ij}}{\partial y_i} + f_i\,, \tag{4}$$

$$m\ddot{z}_i = -\sum_{i\neq j} \frac{\partial V_{ij}}{\partial z_i}\,, \tag{5}$$

where f_i is a random force with zero mean and variance $\langle f_i(0) f_j(t)\rangle = 2mk_BT\Gamma\delta(t)\delta_{ij}$, the temperature is $T = 1.1\,\varepsilon/k_B$ and k_B is the Boltzmann constant. The equations of motion for fluid monomers and wall atoms were integrated using the fifth-order gear-predictor algorithm [35] with a time step $\triangle t = 0.002\,\tau$, where $\tau = \sqrt{m\sigma^2/\varepsilon}$ is the characteristic time of the LJ potential.

Each wall was constructed out of 576 LJ atoms, which formed two (111) layers of the face-centered cubic (fcc) lattice with the density $\rho_w = 1.40\,\sigma^{-3}$. The corresponding nearest-neighbor distance between equilibrium positions of the wall atoms in the xy plane is $d = 1.0\,\sigma$. The dimensions of the Couette cell (xyz) were held fixed to $20.86\,\sigma \times 12.04\,\sigma \times h$, where h is the channel height (see Table I). The MD simulations were performed at a constant density ensemble. The fluid density is defined as a ratio of the total number of monomers to the volume accessible to the fluid, i.e., $0.5\,\sigma_{\rm w}$ away from the fcc lattice planes in the $\hat{z}$ direction.

The range of fluid densities considered in this study is $0.86 \leqslant \rho\,\sigma^3 \leqslant 1.02$. The pressures of the system at equilibrium are given in Table I for each value of the fluid density. Periodic boundary conditions were employed along the $\hat{x}$ and $\hat{y}$ directions parallel to the confining walls.

The wall atoms were attached to their equilibrium fcc lattice positions by the harmonic spring with the potential $V_{sp} = \frac{1}{2}\,\kappa\,r^2$. The spring stiffness $\kappa = 1200\,\varepsilon/\sigma^2$ is large enough so that the mean-square displacement of the wall atoms is less than the Lindemann criterion for melting, i.e., $\langle \delta u^2 \rangle / d^2 \lesssim 0.023$ (see Ref. [36]). In the previous paper on shear flow of simple fluids [37], it was shown that the slope of the rate-dependent slip length remains approximately the same for the thermal walls with $\kappa = 1200\,\varepsilon/\sigma^2$ and rigid fcc walls. The friction term and the random force were also added to the $\hat{x}$, $\hat{y}$ and $\hat{z}$ components of the wall atoms equations of motion

$$m_w\,\ddot{x}_i + m_w\,\Gamma\dot{x}_i \;=\; -\sum_{i\neq j}\frac{\partial V_{ij}}{\partial x_i} - \frac{\partial V_{sp}}{\partial x_i} + f_i\,, \tag{6}$$

$$m_w\,\ddot{y}_i + m_w\,\Gamma\dot{y}_i \;=\; -\sum_{i\neq j}\frac{\partial V_{ij}}{\partial y_i} - \frac{\partial V_{sp}}{\partial y_i} + f_i\,, \tag{7}$$

$$m_w\,\ddot{z}_i + m_w\,\Gamma\dot{z}_i \;=\; -\sum_{i\neq j}\frac{\partial V_{ij}}{\partial z_i} - \frac{\partial V_{sp}}{\partial z_i} + f_i\,, \tag{8}$$

where the mass of the wall atoms is $m_w = 10\,m$ and the summation is performed only over the fluid monomers within the cutoff distance $r_c = 2.5\,\sigma$.

The simulations began with an equilibration period of about $5\times10^4\tau$ with both walls being at rest. Then, the steady-state shear flow was generated by translating the upper wall with a constant velocity U in the $\hat{x}$ direction, while the lower wall always remained stationary (see Fig. 1). The fluid velocity profiles were computed by averaging the instantaneous monomer velocities in the $\hat{x}$ direction within bins of thickness $\Delta z = 0.2\,\sigma$ for a time interval up to $4 \times 10^5\tau$ at the lowest shear rates. The density profiles were averaged for a time period $5 \times 10^4\tau$ within bins of thickness of only $\Delta z = 0.01\,\sigma$ to accurately resolve the fluid structure near the walls [23]. The maximum value of the Reynolds number is $Re \approx 10.5$, which was estimated from the maximum fluid velocity difference across the channel, the shear viscosity, and the channel height. The small values of the Reynolds number correspond to laminar flow conditions even at the highest shear rates considered in this study.

III. RESULTS

A. Fluid density and velocity profiles

The fluid structure in the direction perpendicular to a flat surface usually consists of several distinct layers on the molecular scale [38]. Examples of the averaged monomer density profiles near the lower thermal wall are presented in Fig. 2 for three values of the upper wall velocity. The highest peak is associated with a layer of fluid monomers (each connected to a polymer chain) in contact with the wall atoms. The contact density ρ_c corresponds to the maximum value of the peak. The density oscillations gradually decay away from the wall to a uniform profile with bulk density $\rho = 0.91\,\sigma^{-3}$. The amplitude of the density oscillations is reduced at higher values of the slip velocity.

Figure 3 shows the averaged velocity profiles for the same values of the upper wall speed as in Fig. 2 and the fluid density $\rho = 0.91\,\sigma^{-3}$. For a given U, the relative slip velocity is the same at the upper and lower walls. Surprisingly, the scaled slip velocity is smaller at the intermediate speed of the upper wall $U = 1.0\,\sigma/\tau$. Because of the thermal fluctuations, longer averaging times (up to $4 \times 10^5 \tau$) were required to accurately resolve the fluid velocity profile for $U = 0.05\,\sigma/\tau$. A small curvature in the velocity profile is evident for the largest velocity of the upper wall $U = 5.0\,\sigma/\tau$. The deviation from the linearity might be related to the heating up of the fluid near the walls (see discussion below). The slope of the velocity profile (used for calculation of the slip length and the shear rate) was computed from the central part of the velocity profile excluding the data from the region of about $2\,\sigma$ near the walls.

We comment that at small shear rates, $\dot{\gamma}\tau \lesssim 0.01$, and higher fluid densities, $\rho \gtrsim 1.04\,\sigma^{-3}$, the fluid velocity profiles acquired a pronounced curvature within a distance of about $4\,\sigma$ from the walls. The linearity of the fluid velocity profiles is restored at higher shear rates. This effect will be examined in a separate study.

B. Rate dependence of the slip length and shear viscosity

In the MD study by Thompson and Troian [30] on shear flow of Newtonian liquids past atomically flat surfaces, the slip length was found to increase nonlinearly with the shear rate. The data for different wall densities and weak wall-fluid interactions were fitted well

by the power law function

$$L_s(\dot{\gamma}) = L_s^o \, (1 - \dot{\gamma}/\dot{\gamma}_c)^{-0.5}, \tag{9}$$

where $\dot{\gamma}_c$ and L_s^o are the parameters used for normalization. The rate-dependent slip length in the Poiseuille flow of simple fluids was also well described by the function [Eq. (9)] for incommensurate structures of the liquid/solid interface and weak surface energy [23].

The nonlinear behavior of the slip length can be interpreted in terms of the velocity-dependent shear stress at the wall [39]. By definition, the fluid slip velocity V_s is related to the slip length as $V_s = \dot{\gamma} L_s$. On the other hand, the shear stress through any plane parallel to the walls is the same in the steady-state shear flow, and it is equal to the fluid viscosity multiplied by the shear rate, i.e., $\sigma_{xz} = \mu\dot{\gamma}$. At the liquid/solid interface the viscous shear stress becomes $\sigma_{xz} = kV_s$, where k is the friction coefficient per unit area. The functional form given by Eq. (9) implies that the friction coefficient, $k = \mu/L_s$, can be expressed as a function of the slip velocity as follows:

$$k(V_s) = C_1(\sqrt{C_2 + V_s^2} - V_s), \tag{10}$$

where $C_1 = \mu/2\dot{\gamma}_c(L_s^o)^2$ and $C_2 = (2L_s^o\dot{\gamma}_c)^2$, and μ is the shear-independent viscosity [20, 30].

In the previous MD study [20], it was shown that the slip length increases monotonically with shear rate for polymer melts with short linear chains $N \leqslant 16$. The data for the slip length were well fitted by the power law function given by Eq. (9) for shear rates exceeding $\dot{\gamma} \gtrsim 5 \times 10^{-3}\,\tau^{-1}$. Although the fluid viscosity exhibited a slight shear thinning behavior for chain lengths $N \geqslant 8$, no minimum in the rate dependence of the slip length was observed. In the present study, the shear thinning effect is more pronounced because the polymer melt consists of longer chains and the simulations are performed at higher fluid densities.

Figure 4 shows the rate behavior of the fluid viscosity, which was computed from the Kirkwood relation for the shear stress [31] in steady-state shear flow. In the range of accessible shear rates, the transition from the Newtonian regime to the shear thinning is more evident at lower fluid densities. At higher shear rates, the bulk viscosity approximately follows a power law decay with the exponent -0.37 (see Fig. 4). A similar shear thinning behavior of polymer melts was reported in the previous MD studies [40, 41]. The error bars are larger at lower shear rates because of an increasing role of thermal fluctuations [42].

The dynamic response of the slip length with increasing shear rate is shown in Fig. 5 for the indicated values of the polymer density. The rate dependence of the slip length exhibits

a distinct local minimum, which is followed by a rapid increase at higher shear rates. The minimum is shifted to lower shear rates and becomes more shallow at higher fluid densities. The slip length tends to saturate to a constant value at the lowest shear rates for the fluid density $\rho = 0.86\,\sigma^{-3}$. Typical error bars are included for three points corresponding to the fluid velocity profiles shown in Fig. 3. In the range of shear rates from the local minimum up to the highest $\dot{\gamma}$, the data for the slip length (as well as the ratio L_s/μ) cannot be fitted by the power law function given by Eq. (9). For each value of the fluid density, the highest shear rate corresponds to the maximum sustainable shear stress at the interface [23].

The data for the rate-dependent slip length and fluid viscosity are replotted in Fig. 6 in terms of the friction coefficient at the liquid/solid interface and the slip velocity. The constant value of the friction coefficient at small slip velocities indicates that the ratio of the slip length and viscosity is rate-independent. At higher fluid densities (or pressures), the friction coefficient is larger, and the transition to the power law regime is shifted to smaller slip velocities. The transition point approximately corresponds to the location of the minimum in the shear rate dependence of the slip length shown in Fig. 5. The data for the lowest fluid density $\rho = 0.86\,\sigma^{-3}$ can be fairly well fitted by Eq. (10) [see Fig. 6], but the fit becomes worse at higher fluid densities (not shown). The simulation results indicate that the nonmonotonic rate behavior of the slip length for polymer melts can be ascribed to the velocity dependence of the friction coefficient, which undergoes a transition from a nearly constant value to a decreasing function of the slip velocity.

Furthermore, the data for different fluid densities can be collapsed onto a single master curve by scaling both axes (see Fig. 7). The values of the normalization parameters for the friction coefficient and the slip velocity are listed in the inset. The decay at large slip velocities approximately follows the power law function with the exponent -0.7 (see Fig. 7). The onset of the power law decay depends on the polymer density and might occur when the time scale of the in-plane diffusion of the fluid monomers over the lattice spacing d is comparable to d/V_s. We also note that the data for the viscosity and slip length at the interface between a polymer melt (with linear chains $N = 20$ and density $\rho = 0.88\,\sigma^{-3}$) and a rigid fcc wall (with density $\rho_w = 1.94\,\sigma^{-3}$ and $\varepsilon_{\rm wf} = \varepsilon$) can be normalized to follow the master curve shown in Fig. 7 [43].

C. Analysis of the fluid structure in the first layer

The surface induced order in the adjacent fluid layer is described by the structure factor at the reciprocal lattice vectors of the crystal wall [15]. The structure factor is defined as

$$S(\mathbf{k}) = \frac{1}{N_\ell} \Big| \sum_j e^{i\,\mathbf{k}\cdot\mathbf{r}_j} \Big|^2, \tag{11}$$

where $\mathbf{r}_j = (x_j, y_j)$ is the position vector of the j-th monomer and the summation is performed over N_ℓ monomers within the first layer. The friction force between a layer of adsorbed monomers and a solid substrate is proportional to the peak value of the in-plane structure factor estimated at the first reciprocal lattice vector [44, 45]. Previous MD studies of simple fluids have also reported a strong correlation between the slip length (which is inversely proportional to the friction coefficient at the liquid/solid interface) and the surface induced order in the first fluid layer [15, 16, 23].

Figure 8 shows the averaged structure factor in the first fluid layer moving with a constant velocity against the stationary lower wall. The circular ridge at the wavevector $|\mathbf{k}| \approx 2\pi/\sigma$ is attributed to the short-range ordering of the fluid monomers. The periodic potential of the crystalline substrate induces several sharp peaks in the fluid structure factor, which are reduced at higher slip velocities. The first reciprocal lattice vector in the direction of shear flow is $\mathbf{G}_1 = (7.23\,\sigma^{-1}, 0)$. Although the nearest-neighbor distance between equilibrium lattice sites in the xy plane is equal to the diameter of the LJ monomers, the surface induced order in the first fluid layer is frustrated by the topological constraints associated with packing of polymer chains near the surface.

In the recent MD study on shear flow of simple fluids past rigid fcc walls [23], it was shown that the slip length scales according to

$$L_s \sim \left[\, T_1 / S(\mathbf{G}_1)\, \rho_c \right]^{1.44}, \tag{12}$$

where $\mathbf{G}_1$ is the the first reciprocal lattice vector, T_1 and ρ_c are the temperature and the contact density of the first fluid layer respectively. This relation was found to hold in a wide range of shear rates and for weak wall-fluid interactions $0.3 \leqslant \varepsilon_{\rm wf}/\,\varepsilon \leqslant 1.1$. It is expected, however, that the scaling relation given by Eq. (12) is not valid at higher surface energies because the first fluid layer is locked to the solid wall and, as a consequence, the slip length is negative [15]. Note that the surface induced peaks in the structure factor are much higher

for polymers (see Fig. 8) than for simple fluid [23]. Since the viscosity is independent of shear rate for simple fluids, the scaling relation Eq. (12) also predicts the dependence of the friction coefficient on microscopic parameters of the adjacent fluid layer.

We computed the parameters entering Eq. (12) in the first fluid layer for the polymer melt. The fluid temperature was estimated from the kinetic energy

$$k_B T = \frac{m}{3N} \sum_{i=1}^{N} [\dot{\mathbf{r}}_i - \mathbf{v}(\mathbf{r}_i)]^2, \tag{13}$$

where $\dot{\mathbf{r}}_i$ is the instantaneous velocity of the fluid monomer and $\mathbf{v}(\mathbf{r}_i)$ is the local average flow velocity. Averaged temperature profiles are shown in Fig. 9 for the same flow conditions as in Figs. 2 and 3. At low shear rates $\dot{\gamma} \lesssim 0.01\,\tau^{-1}$, the fluid temperature is equal to its equilibrium value of $T = 1.1\,\varepsilon/k_B$ determined by the Langevin thermostat. As in the case of simple fluids [23, 37], with further increase of the shear rate, the polymer melt heats up and the temperature profile becomes non-uniform across the channel. The fluid temperature is higher near the walls because of the large slip velocity, which is comparable to the thermal velocity, $v_T^2 = k_B T/m$, at high shear rates. The non-uniform temperature distribution might be related to the slight curvature in the velocity profile for the top wall speed $U = 5.0\,\sigma/\tau$ shown in Fig. 3. We can also notice that at high shear rates, the temperature in the $\hat{y}$ direction, in which the Langevin thermostat is applied, is slightly smaller than its value in the $\hat{x}$ and $\hat{z}$ directions (see inset of Fig. 9). This difference implies that the kinetic energy in the $\hat{y}$ direction dissipates faster than the energy transfer from the other directions. In principle, it is important to investigate whether the choice of the thermostat, e.g. dissipative particle dynamics thermostat, has an effect on the velocity and temperature profiles at high shear rates [46]. In the present study, the temperature in the first fluid layer was computed from

$$T_1 = \int_{z_0}^{z_1} T(z)\rho(z)dz \,/\, \int_{z_0}^{z_1} \rho(z)dz, \tag{14}$$

where the limits of integration ($z_0 = -14.4\,\sigma$ and $z_1 = -13.8\,\sigma$) are given by the width of the first peak in the density profile (e.g. see Fig. 2).

The ratio of the slip length to viscosity is plotted in Fig. 10 as a function of $T_1/[S(\mathbf{G}_1)\,\rho_c]$ for different fluid densities and shear rates. Except for higher densities at low shear rates, the data collapse onto a single curve, which approximately follows the power law function with a slope of 0.9 (see Fig. 10). Although the slope is different from the value 1.44 reported

for simple fluids [23], it is remarkable that the same combination of parameters determines the boundary conditions for both polymer melts and simple fluids. The simulation results also show that for each value of the fluid density, the number of fluid monomers in the first layer $N_\ell = S(0)$ decreases by about 4% at the highest shear rates. The same data for the slip length and viscosity are replotted as a function of the variable $S(0)/\left[S(\mathbf{G}_1)\,\rho_c\right]$ in Fig. 11. The collapse of the data is consistent with the previous results for the rate-independent slip length at the interface between simple fluids and crystalline walls [15]. The correlation between the friction coefficient and the fluid structure in the adjacent layer presented in Figs. 10 and 11 suggests a possible existence of a general functional relation between the slip length, shear rate and polymer density.

IV. CONCLUSIONS

In this paper, the rate dependence of the slip length in the shear flow of polymer melts past atomically smooth, thermal surfaces was studied using molecular dynamics simulations. For weak wall-fluid interactions, the slip length passes through a minimum as a function of shear rate and then increases rapidly at higher shear rates. The nonlinear rate dependence of the slip length was analyzed in terms of the dynamic friction at the liquid/solid interface. In a wide range of fluid densities, the friction coefficient (the ratio of the shear viscosity and the slip length) undergoes a universal transition from a constant value to the power law decay as a function of the slip velocity. The simulation results for polymer melts confirm the previous findings for simple fluids [23] that the surface induced structure and the contact density of the adjacent fluid layer are crucial factors for determining the value of the friction coefficient.

Future research will be focused on the rate dependence of the slip length for higher fluid densities and entangled polymer melts.

Acknowledgments

Financial support from the Michigan State University Intramural Research Grants Program is gratefully acknowledged. Computational work in support of this research was per-

formed at Michigan State University's High Performance Computing Facility.

---

[1] L. Bocquet and J.-L. Barrat, Soft Matter **3**, 685 (2007).

[2] N. V. Churaev, V. D. Sobolev, and A. N. Somov, J. Colloid Interface Sci. **97**, 574 (1984).

[3] K. B. Migler, H. Hervet, and L. Leger, Phys. Rev. Lett. **70**, 287 (1993).

[4] J. Baudry, E. Charlaix, A. Tonck, and D. Mazuyer, Langmuir **17**, 5232 (2001).

[5] V. Mhetar and L. A. Archer, Macromolecules **31**, 6639 (1998).

[6] R. G. Horn, O. I. Vinogradova, M. E. Mackay, and N. Phan-Thien, J. Chem. Phys. **112**, 6424 (2000).

[7] K. M. Awati, Y. Park, E. Weisser, and M. E. Mackay, J. Non-Newton. Fluid Mech. **89**, 117 (2000).

[8] Y. Zhu and S. Granick, Phys. Rev. Lett. **87**, 096105 (2001).

[9] C. H. Choi, K. J. A. Westin, and K. S. Breuer, Phys. Fluids **15**, 2897 (2003).

[10] J. Sanchez-Reyes and L. A. Archer, Langmuir **19**, 3304 (2003).

[11] Y. Zhu and S. Granick, Phys. Rev. Lett. **88**, 106102 (2002).

[12] O. I. Vinogradova and G. E. Yakubov, Phys. Rev. E **73**, 045302(R) (2006).

[13] T. Schmatko, H. Hervet, and L. Leger, Langmuir **22**, 6843 (2006).

[14] J. Koplik, J. R. Banavar, and J. F. Willemsen, Phys. Fluids A **1**, 781 (1989).

[15] P. A. Thompson and M. O. Robbins, Phys. Rev. A **41**, 6830 (1990).

[16] J.-L. Barrat and L. Bocquet, Faraday Discuss. **112**, 119 (1999).

[17] J.-L. Barrat and L. Bocquet, Phys. Rev. Lett. **82**, 4671 (1999).

[18] A. Jabbarzadeh, J. D. Atkinson, and R. I. Tanner, J. Chem. Phys. **110**, 2612 (1999).

[19] M. Cieplak, J. Koplik, J. R. Banavar, Phys. Rev. Lett. **86**, 803 (2001).

[20] N. V. Priezjev and S. M. Troian, Phys. Rev. Lett. **92**, 018302 (2004).

[21] T. M. Galea and P. Attard, Langmuir **20**, 3477 (2004).

[22] N. V. Priezjev, A. A. Darhuber, and S. M. Troian, Phys. Rev. E **71**, 041608 (2005).

[23] N. V. Priezjev, Phys. Rev. E **75**, 051605 (2007).

[24] P. A. Thompson, M. O. Robbins, and G. S. Grest, Israel Journal of Chemistry **35**, 93 (1995).

[25] R. Khare, J. J. de Pablo, and A. Yethiraj, Macromolecules **29**, 7910 (1996).

[26] A. Koike and M. Yoneya, J. Phys. Chem. B **102**, 3669 (1998).

[27] X. Zhou, D. Andrienko, L. Delle Site, and K. Kremer, J. Chem. Phys. **123**, 104904 (2005).

[28] C. Pastorino, K. Binder, T. Kreer, and M. Muller, J. Chem. Phys. **124**, 064902 (2006).

[29] S. Barsky and M. O. Robbins, Phys. Rev. E **63**, 021801 (2001).

[30] P. A. Thompson and S. M. Troian, Nature (London) **389**, 360 (1997).

[31] R. B. Bird, C. F. Curtiss, R. C. Armstrong, and O. Hassager, *Dynamics of Polymeric Liquids* 2nd ed. (Wiley, New York, 1987).

[32] K. Kremer and G. S. Grest, J. Chem. Phys. **92**, 5057 (1990).

[33] G. S. Grest and K. Kremer, Phys. Rev. A **33**, 3628 (1986).

[34] M. Tsige and G. S. Grest, J. Chem. Phys. **120**, 2989 (2004).

[35] M. P. Allen and D. J. Tildesley, *Computer Simulation of Liquids* (Clarendon, Oxford, 1987).

[36] J. L. Barrat and J. P. Hansen, *Basic concepts for simple and complex liquids* (Cambridge University Press, Cambridge, 2003).

[37] N. V. Priezjev, J. Chem. Phys. **127**, 144708 (2007).

[38] J. N. Israelachvili, *Intermolecular and Surface Forces*, 2nd ed. (Academic Press, San Diego, 1992).

[39] M. O. Robbins, Nature (London) **389**, 331 (1997).

[40] Z. Xu, J. J. de Pablo, and S. Kim, J. Chem. Phys. **102**, 5836 (1995).

[41] J. T. Bosko, B. D. Todd, and R. J. Sadus, J. Chem. Phys. **121**, 12050 (2004).

[42] Z. Xu, R. Khare, J. J. de Pablo, and S. Kim, J. Chem. Phys. **106**, 8285 (1997).

[43] A. Niavarani and N. V. Priezjev, unpublished (cond-mat/0801.3828).

[44] E. D. Smith, M. O. Robbins, and M. Cieplak, Phys. Rev. B **54**, 8252 (1996).

[45] M. S. Tomassone, J. B. Sokoloff, A. Widom, J. Krim, Phys. Rev. Lett. **79**, 4798 (1997).

[46] C. Pastorino, T. Kreer, M. Muller, and K. Binder, Phys. Rev. E **76**, 026706 (2007).

Figures

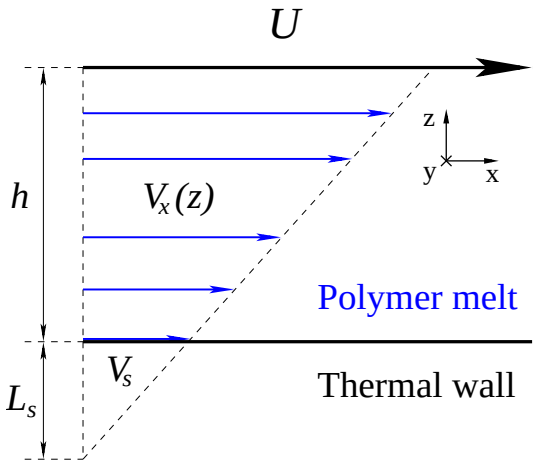

FIG. 1: (Color online) A schematic representation of the steady-state shear flow in the Couette cell. The upper wall is translated with a constant velocity U in the $\hat{x}$ direction. The fluid slip velocity is determined from the relation $V_s = \dot{\gamma} L_s$, where $\dot{\gamma}$ is the slope of the velocity profile and L_s is the slip length.

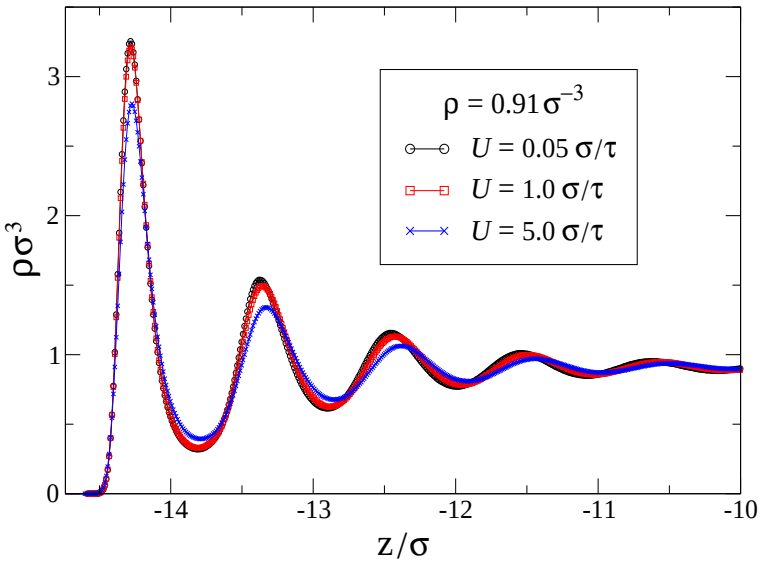

FIG. 2: (Color online) Averaged fluid density profiles near the stationary thermal wall with $\kappa = 1200\,\varepsilon/\sigma^2$ and $\varepsilon_{\rm wf}/\varepsilon = 0.9$. The velocities of the upper wall are tabulated in the inset. The fluid density in the center of the cell is $\rho = 0.91\,\sigma^{-3}$. The left vertical axis denotes the position of the liquid/solid interface at $z = -14.74\,\sigma$.

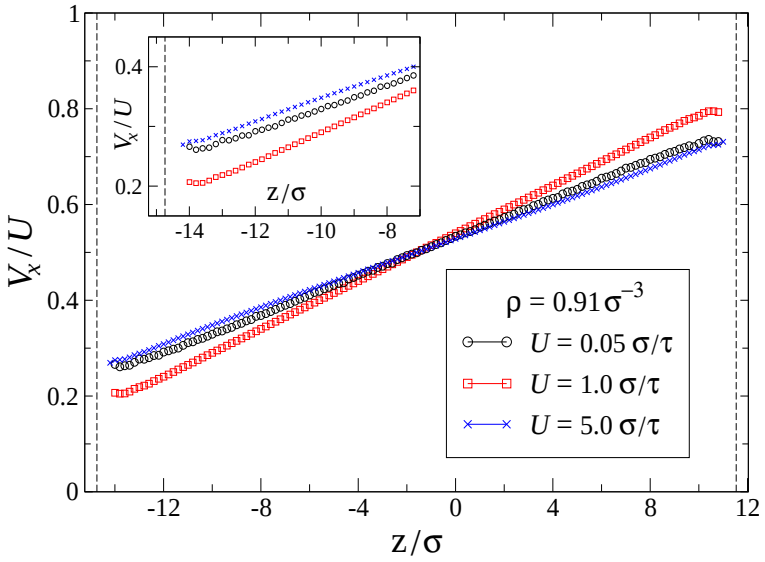

FIG. 3: (Color online) Average normalized velocity profiles, V_x/U, for the indicated values of the upper wall velocity U and the fluid density $\rho = 0.91\,\sigma^{-3}$. Vertical axes denote the position of the fcc lattice planes at $z = -15.24\,\sigma$ and $z = 12.03\,\sigma$. The dashed lines indicate the location of liquid/solid interfaces at a distance $0.5\,\sigma_{\rm w}$ away from the fcc lattice planes, i.e., $z = -14.74\,\sigma$ and $z = 11.53\,\sigma$. The inset shows the same data near the lower wall.

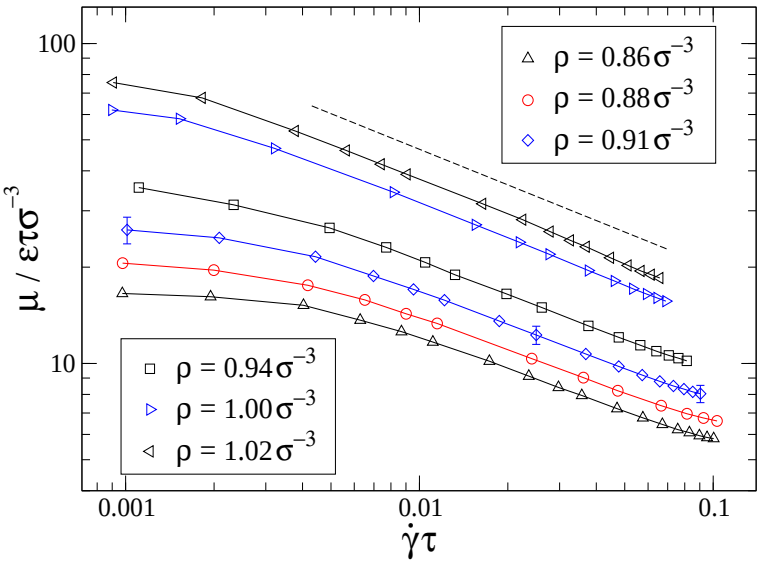

FIG. 4: (Color online) Behavior of the fluid viscosity $\mu/\varepsilon\tau\sigma^{-3}$ as a function of shear rate for the tabulated values of the polymer density. The straight dashed line with a slope -0.37 is shown for reference. Solid curves are a guide for the eye.

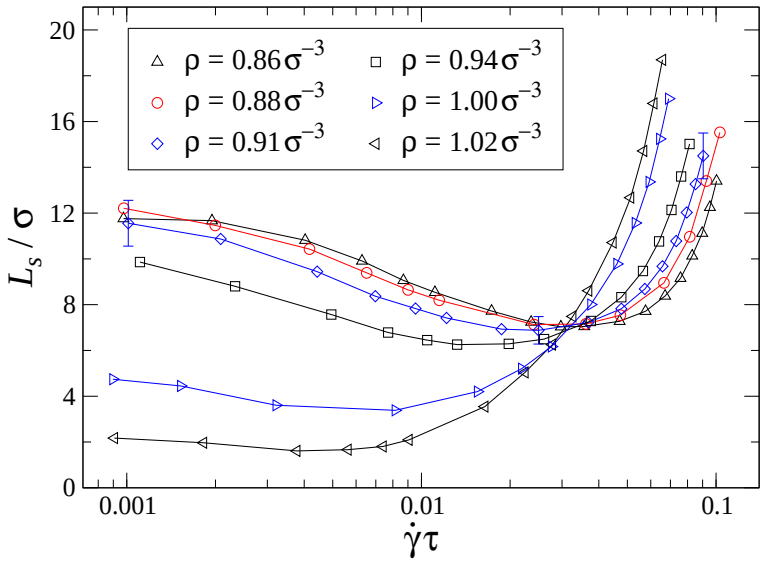

FIG. 5: (Color online) Slip length L_s/σ as a function of the shear rate for the polymer melt with linear chains $N = 20$. Solid curves are a guide for the eye.

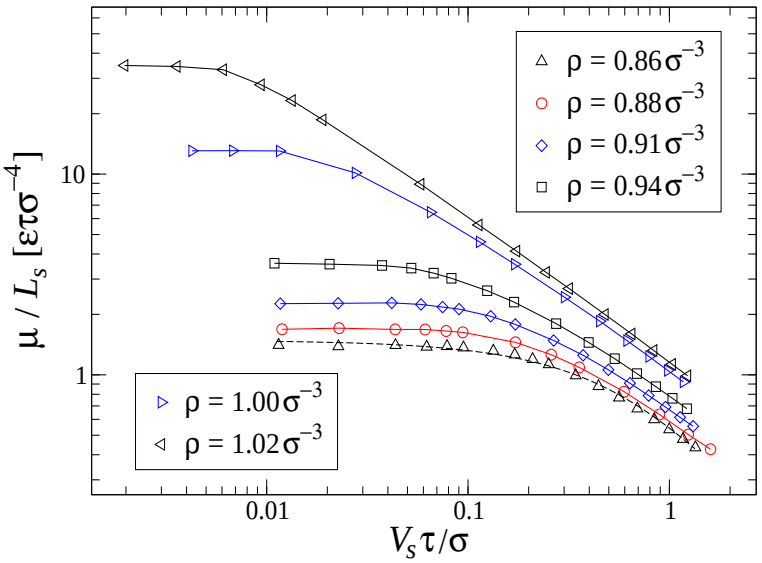

FIG. 6: (Color online) Log-log plot of the friction coefficient, $k = \mu/L_s$, as a function of the slip velocity for the indicated values of the fluid density. The dashed curve is the best fit to Eq. (10) with $C_1 = 1.77\, m\sigma^{-3}$ and $C_2 = 0.71\, \sigma^2\tau^{-2}$. Solid curves are a guide for the eye.

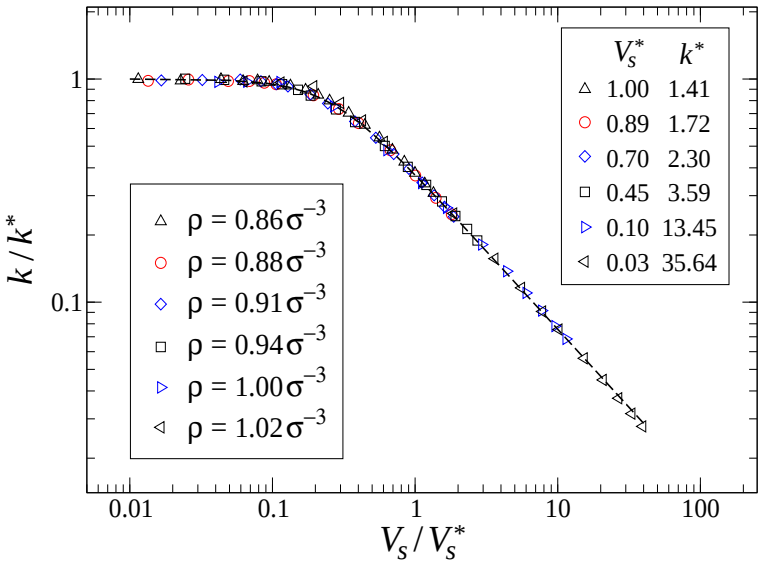

FIG. 7: (Color online) Master curve for the friction coefficient as a function of the slip velocity. The same data as in Fig. 6. The values of the friction coefficient k^* [$\varepsilon\tau\sigma^{-4}$] and the slip velocity V_s^* [σ/τ] used for normalization of the data are shown in the inset. The dashed line $y = [1 + (4x)^2]^{-0.35}$ is plotted for reference.

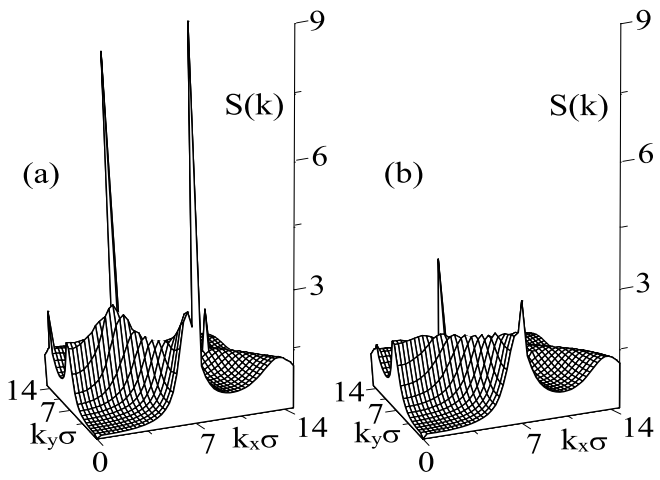

FIG. 8: Structure factor $S(k_x, k_y)$ in the first fluid layer for the fluid density $\rho = 0.91\,\sigma^{-3}$. The upper wall velocity is $U = 0.05\,\sigma/\tau$ (a) and $U = 5.0\,\sigma/\tau$ (b). The same flow conditions as in Fig. 3.

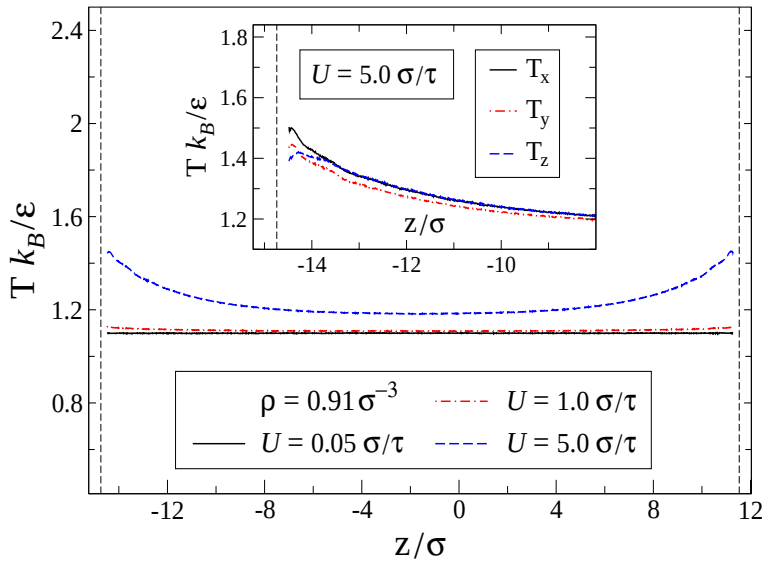

FIG. 9: (Color online) Temperature profiles for the indicated values of the upper wall speed U and the fluid density $\rho = 0.91\,\sigma^{-3}$. Vertical dashed lines denote the position of the liquid/solid interface. The inset shows the $\hat{x}$, $\hat{y}$ and $\hat{z}$ components of the temperature profile near the stationary lower wall when the velocity of the upper wall is $U = 5.0\,\sigma/\tau$.

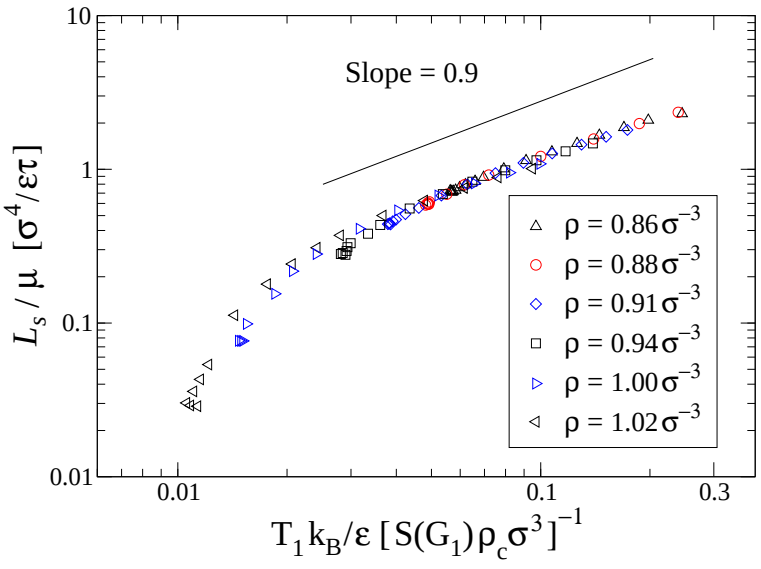

FIG. 10: (Color online) Log-log plot of L_s/μ as a function of the ratio $T_1 k_B/\varepsilon\,[S(\mathbf{G}_1)\,\rho_c\,\sigma^3]^{-1}$ for the indicated values of the polymer density. The solid line with a slope 0.9 is plotted for reference.

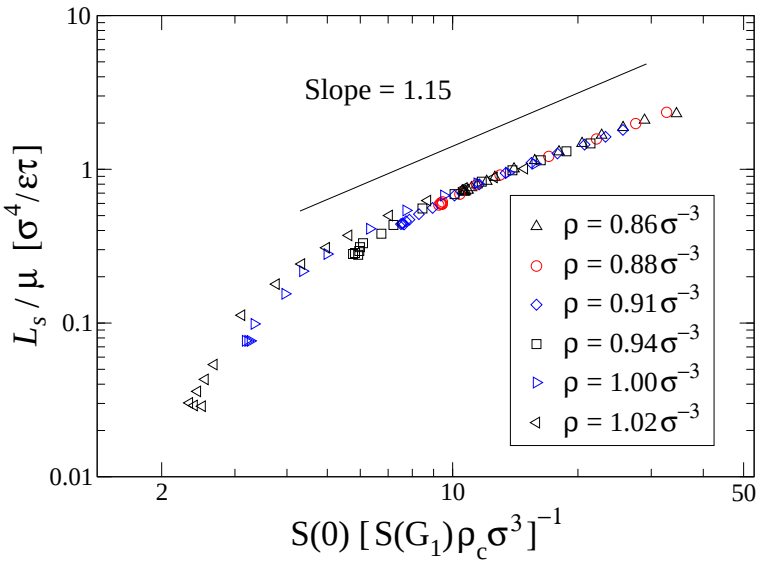

FIG. 11: (Color online) Log-log plot of the ratio L_s/μ as a function of the variable $S(0)/\left[S(\mathbf{G}_1)\,\rho_c\,\sigma^3\right]$. The values of the fluid density are tabulated in the inset. The same data as in Fig. 10. The straight solid line with a slope 1.15 is plotted as a reference.

Tables

TABLE I: The fluid pressure P at equilibrium, i.e., with the stationary upper wall, and the channel height h (defined as a distance between the inner fcc planes) as a function of the fluid density.

$\rho\,[\,\sigma^{-3}]$	0.86	0.88	0.91	0.94	1.00	1.02
$P\,[\,\varepsilon\,\sigma^{-3}]$	0.0	0.5	1.0	2.0	4.0	5.0
$h\,[\sigma]$	28.93	28.18	27.27	26.32	24.85	24.36